



Fabrication and electrochemical evaluation of micro-supercapacitors prepared by direct laser writing on free-standing graphite oxide paper

Rajesh Kumar ^{a,*}, Ednan Joanni ^b, Raluca Savu ^c, Matheus S. Pereira ^d, Rajesh K. Singh ^e, Carlos J.L. Constantino ^d, Lauro T. Kubota ^f, Atsunori Matsuda ^a, Stanislav A. Moshkalev ^{c,**}

^a Department of Electrical and Electronic Information Engineering, Toyohashi University of Technology, 1-1 Hibarigaoka, Tempaku-cho, Toyohashi, Aichi, 441-8580, Japan

^b Centre for Information Technology Renato Archer (CTI), Campinas, 13069-901, Brazil

^c Centre for Semiconductor Components and Nanotechnology (CCS Nano), University of Campinas (UNICAMP), Campinas, 13083-870, Sao Paulo, Brazil

^d Faculty of Science and Technology, Department of Physics, São Paulo State University, Presidente Prudente, 19060-900, Sao Paulo, Brazil

^e School of Physical & Material Sciences, Central University of Himachal Pradesh (CUHP), Kangra, Dharamshala, HP, 176215, India

^f Department of Analytical Chemistry, Institute of Chemistry, University of Campinas (UNICAMP), P.O. Box 6154, Campinas, 13084-974, Sao Paulo, Brazil

ARTICLE INFO

Article history:

Received 16 October 2018

Received in revised form

3 May 2019

Accepted 4 May 2019

Available online 9 May 2019

Keywords:

GO paper

Pulsed laser

Direct laser writing

μ -supercapacitors

Areal capacitance

Cycling stability

ABSTRACT

This article presents results of a pulsed UV laser method for the simultaneous reduction of graphite oxide (GO) and patterning of reduced graphene oxide (rGO). This direct laser writing method was applied to the fabrication of graphene-based, in-plane interdigitated micro-supercapacitors (μ -SCs), prepared on free-standing GO paper (10 μ m thick). The electrochemical performance of μ -SCs was studied using two different electrolytes (KOH and NaCl). The results from cyclic voltammetry measurements exhibited typical electrical double layer behavior, with specific capacitances of 9.3 μ F/cm² and 13.8 μ F/cm² (at a scan rate of 10 mV/s) for KOH and NaCl electrolytes, respectively. The μ -SCs exhibited good performance, with retention of 95% of the original capacitance values after 3400 charge-discharge cycles. When compared to devices obtained by conventional lithographic techniques, the laser fabrication of planar μ -SCs is faster, cost-effective and scalable. We believe this one-step and environmentally friendly laser-assisted method to be a good alternative for the fabrication of flexible energy storage devices.

© 2019 Elsevier Ltd. All rights reserved.

1. Introduction

Among the various alternative energy storage technologies, supercapacitors (SCs) are one of the most promising electrochemical energy storing devices [1–7]. Flexible SCs have lately attracted tremendous attention due to the many advantages such as their tailored size, light weight and high energy density capacity [8–10]. However, recent advances in SCs have led to the development of micro-SCs (μ -SCs), further reducing the device volume and facilitating easy integration into micro devices [11]. Excellent flexibility, high rate capability, high power density, high energy density and long cycle life are potential advantages of μ -SCs [12,13].

Several techniques have been reported for fabrication/

patterning of μ -SCs using processes like photolithography [14], hotwire chemical vapor deposition [15], pencil drawing [16], electrochemical deposition and post annealing [17], template plasma etching [18], layer-by-layer printing [19], electrophoretic deposition [20], inkjet printing [21], screen printing [22], selective wetting-induced fabrication [23] and microfluidic etching [24]. Also, μ -SCs have been designed on different substrates, using various electrode materials, such as conducting polymers [25], carbonaceous materials [26] and metal oxides [27]. However, these fabrication methods for μ -SCs have several disadvantages that hinder their widespread adoption, since they require expensive raw materials or make use of toxic chemicals. The processing methods are also complex and time-consuming, raising the fabrication costs. In spite of the many alternatives already proposed for SC fabrication, there are still some challenges that must be overcome in order to achieve superior performance in all of the main characteristics.

Laser based techniques rely on the optically induced local heating at the focusing area (laser spot), allowing the reduction of

* Corresponding author.

** Corresponding author.

E-mail addresses: rajeshbhu1@gmail.com, rajeshbhug@gmail.com (R. Kumar), stanisla@unicamp.br (S.A. Moshkalev).

GO paper only in the regions exposed to the laser [28]. By moving the laser spot across the sample surface, this technique allows one to “write” the desired rGO patterns. Laser-based techniques offer an easy fabrication method for interdigitated electrodes in μ -SCs [29]. Direct laser writing seems to have a vast potential for quick and scalable synthesis of impurity-free graphene patterns on graphite oxide (GO) paper. This technique has been attracting a large amount of interest because it provides a fast and simple preparation route, suitable for application to flexible substrates. Also, direct laser-writing techniques are appropriate for engineering multiple μ -SC shapes within short periods of time, without the need for masking and transfer operations. Direct laser writing on different carbon-containing materials have been used for building high-performance, flexible μ -SCs [30,31]. Recently, Kumar et al. have reported direct laser writing on thin GO films for interdigitated μ -SCs [32,33]. The authors varied the laser-processing parameters (scan speed, laser power and pulse frequency) and film thickness, performing electrochemical analysis with different combinations of electrolytes. Further information about laser-material interactions and related technical details involved in direct laser writing can be found in a previous review article [34], as well as in other recently published articles [34–37].

Herein, we demonstrate the fabrication of interdigitated μ -SCs using direct laser writing on free-standing GO paper (10 μ m thick). Complete local reduction of GO paper by one-step laser writing has been made possible without resorting to high temperature processing. The electrochemical performance of μ -SCs was analyzed using two different types of electrolytes (KOH and NaCl). The fabricated μ -SCs show good areal capacitance, with excellent cycling stability.

2. Experimental

2.1. Synthesis of GO suspensions

GO was synthesized using modified Hummer's method [38]. Graphite flakes (1.0 g) were mixed into a rounded bottom flask containing H_2SO_4 (100 ml, 98.0%) under stirring (at $<40^\circ\text{C}$). Afterwards, KMnO_4 (2 g) was slowly added, generating a characteristic green color attributed to the oxidizing agent Mn_2O_7 [39,40]. After completing the oxidation process, ultrapure water (250 ml, in ice form) was added and subsequently H_2O_2 (4.0 ml, 30% vol.) was poured to deplete the residual KMnO_4 present. The resulting mixture was centrifuged and washed with DI water and 5% HCl (v/v) solution. The product was washed several times using de-ionized water in order to remove acidic species. Finally, the GO dispersed in water was purified by dialysis for one week, using cellulose tubular membranes, for complete removal of remaining salt impurities. The resulting homogeneous suspension of GO (2.1 mg/ml) was stored for preparation of free-standing GO paper.

2.2. Fabrication of free-standing GO papers

The GO was vacuum-filtered from the suspension through a 4.7 cm diameter Millipore (type HA) membrane with pore sizes of 0.45 μ m. After filtration and drying in air, the GO papers were peeled off from the membrane filters. The resulting free-standing flexible samples were used to fabricate the final μ -SCs devices using direct laser writing. Fig. 1 shows a schematic representation of the preparation of free-standing GO papers from GO suspension and the process of direct laser writing for μ -SCs.

2.3. Fabrication of μ -SCs on free-standing GO papers

The laser treatment system used for direct writing of the

interdigitated electrodes is composed of computer-controlled linear stages in an x-y configuration with z focus adjustment, using custom-built software for pattern design and movement control, and a diode-pumped solid-state (DPSS) laser. The ultraviolet (UV) laser (Pulseo 355-20, Spectra-Physics) is a Nd:YVO₄ pulsed laser ($\lambda = 355$ nm) with pulse duration of 20 ns, minimum spot size of 10 μ m and 20 W maximum UV power. The GO paper was placed on the x-y controlled table under the stationary laser source and the interdigitated electrodes were drawn through direct laser reduction of the GO paper in air. The three most important variables in the process of direct laser reduction are the laser power, scanning speed and focusing. After optimization of these parameters, it was concluded that a laser power of 325 mW and a scan speed of 2 mm/s were suitable for complete reduction of the GO paper across the entire thickness [32]. The as fabricated μ -SCs contained 19 parallel pairs of rGO electrodes with an area of 1.14 cm² (19 mm length and 6 mm width). Each linear, uniformly reduced electrode “finger” was 5 mm long and 100 μ m wide, with a spacing of 400 μ m (unreduced GO) between fingers. Two rGO contact pads 2.5×2.5 mm² were drawn at the end of each electrode, providing convenient contacts for the electrochemical measurements [33].

2.4. Characterization

The 10 μ m thick, pristine GO paper and the laser-reduced portions were characterized using optical microscopy, scanning electron microscopy (SEM) and Raman spectroscopy. Optical microscopic observations were carried out on an Olympus MX51-F Microscope under reflectance mode. Electron microscopy was performed on a FEG SEM with energy-dispersive X-ray probe from FEI Company (Dual Beam FIB/FEG model Nova 200) using electron beam currents in the 0.4–1.6 nA range and 5–10 kV energy. Energy dispersive X-ray spectroscopy (EDS) analysis was used to assess the changes in the oxygen-containing functional groups on the surface of GO after the laser treatments. In order to avoid charging the insulating GO paper, a fine metallic grounding contact was clamped onto one corner of the sample during SEM characterization. Raman measurements were carried out using a NT-MDT NTEGRA Spectra spectrometer with a 473 nm laser.

2.5. Electrochemical measurements

Cyclic voltammetry (CV), galvanostatic charge/discharge and electrochemical impedance spectroscopy (EIS) of μ -SCs were performed with a CHI660D electrochemical workstation (Shanghai Chenhua) using a two electrode system with two different kinds of electrolytes (KOH and NaCl) with the same molarity (1 M). The CV measurement of μ -SCs was carried out in the potential window between 0 and 0.8 V with various scan rates in the range between 10 and 600 mV/s. The EIS was conducted in the frequency range between 0.1 Hz and 100 kHz with a signal amplitude of 5 mV.

3. Results and discussion

Fig. 2 (a,b) shows the optical images of as-synthesized, free-standing, flexible/foldable and semi-transparent GO paper after filtration and drying in air. The GO paper displays a uniform yellow-brown color when examined under white light. Fig. 2c shows a GO paper containing the laser-written interdigitated electrodes of two μ -SCs on its surface.

The morphologies of the as-prepared GO paper and of the rGO electrodes generated by laser writing were further observed by SEM. The GO paper exhibits nearly flat surfaces (Fig. 3a) but a few individual, well-defined GO wrinkles were induced during the GO

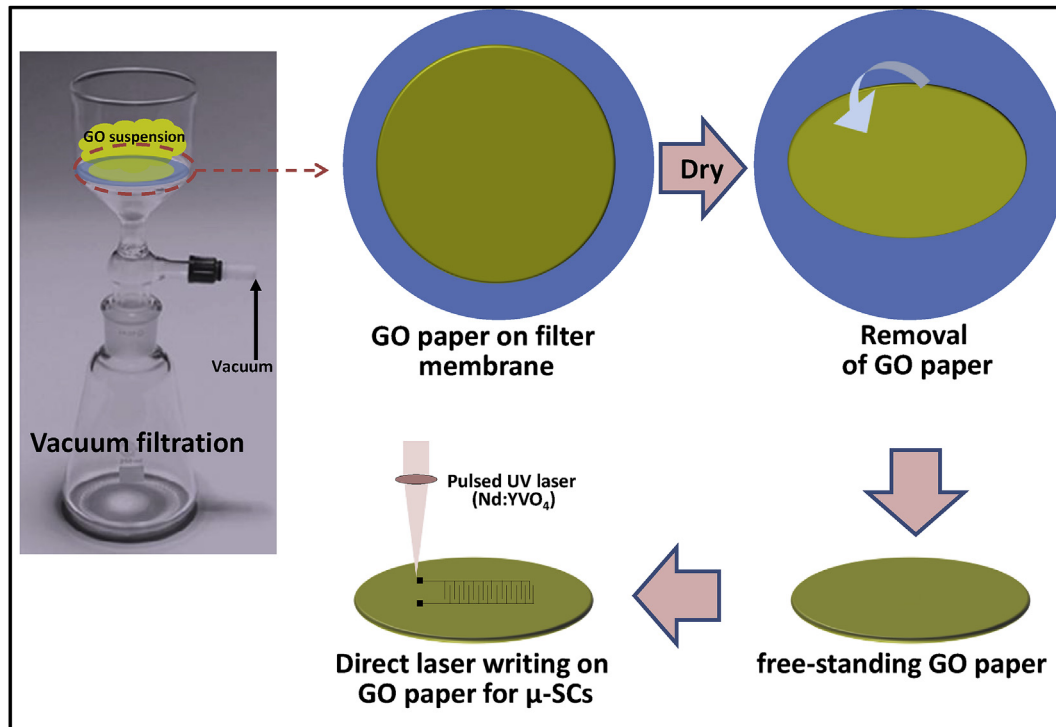


Fig. 1. Schematic illustration of the processes for preparation of free-standing and flexible GO paper for direct laser writing of μ -SCs.

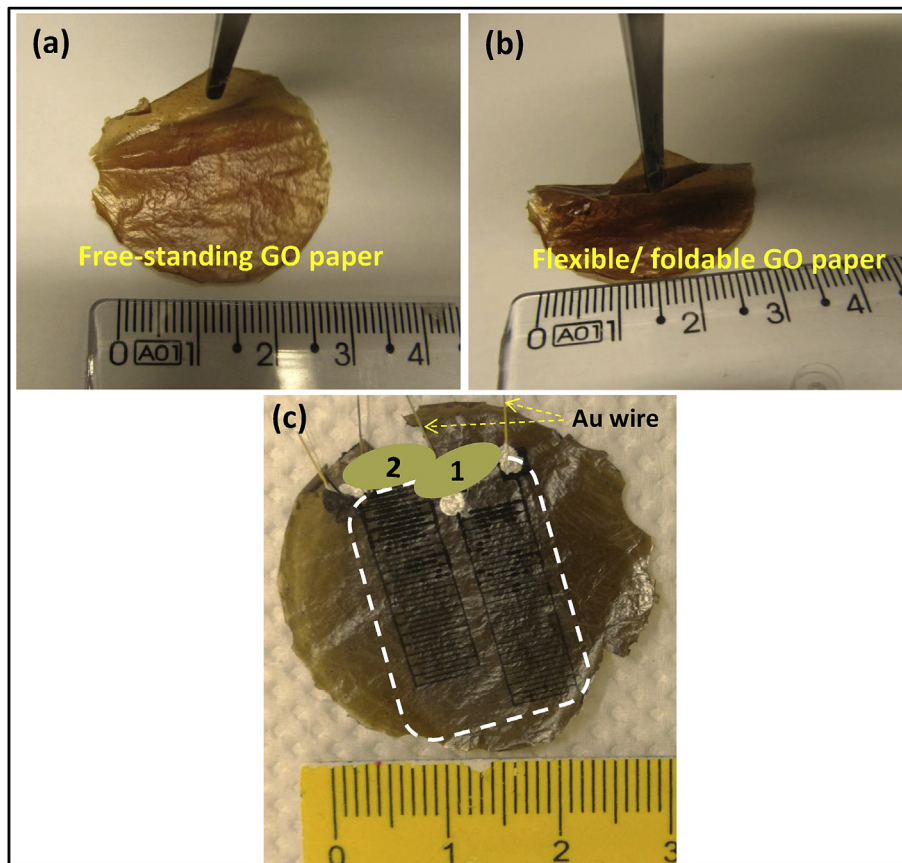


Fig. 2. Optical images of GO paper and μ -SCs. (a,b) free-standing, flexible/foldable GO paper. (c) Laser-written μ -SCs on free-standing GO paper with interdigitated electrodes on 1.14 cm^2 .

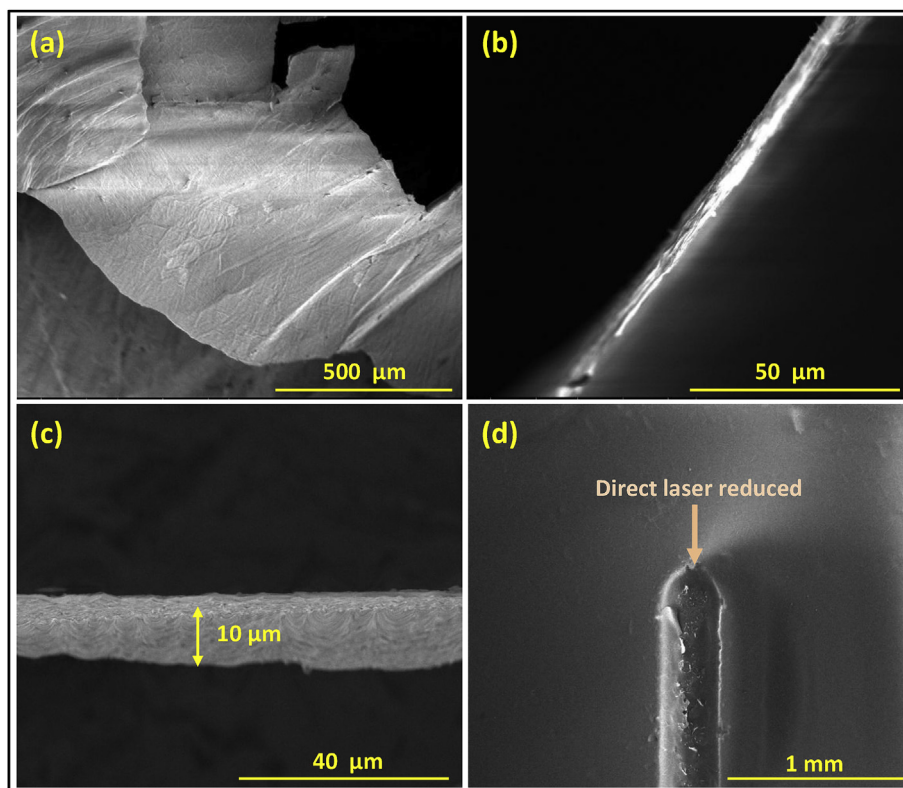


Fig. 3. SEM images of (a) GO paper, (b,c) thickness/edge of GO paper and (d) tip of laser-reduced line from interdigitated electrodes written on GO paper.

filtration process. From the layered structure seen in the cross-sectional images (Fig. 3b and c), the thickness of the GO membrane was determined to be approximately 10 μm . Fig. 3d reveals the tip of a single electrode line with thickness of ~ 0.36 mm on the surface of GO paper. After laser reduction, the surfaces of GO swell due to the formation of a porous open structure.

Fig. 4 shows an optical image of lines drawn by laser on GO paper in order to optimize the processing conditions for writing $\mu\text{-SCs}$. The photograph shows that GO paper treated with different

values of laser power (at fixed scan speed) show different optical contrasts and colors, resulting from different degrees of reduction by the laser and from the surface profiles. The surface relief is generated either from ablation (excessive laser energy breaking C–C bonds) or from local swelling due to the increase in interplanar distances resulting from desorption of chemical groups attached to GO. The result of laser treatment is very sensitive to changes in the processing conditions. The figure shows that even small laser power variations can produce ablation, partial reduction, reduction with ablation etc. (a = 365 mW; b = 310 mW; c = 340 mW; d = 335 mW and e = 325 mW). A laser power value of 325 mW generated complete GO reduction without ablation and it was deemed suitable for direct laser writing of $\mu\text{-SCs}$. The optimization was simplified because starting parameter ranges (for laser power, scan speed and focusing) had already been established in our previous studies using other forms of GO [31,32].

The elemental analyses of GO paper and of the laser-reduced regions of the GO paper (converted into rGO) are shown, together with the EDS spectra, in Fig. 5. The EDS results show that the GO paper contains only carbon and oxygen, without any impurities. The concentrations of carbon and oxygen in the GO sample were 55.53 wt% and 44.47 wt%, respectively (Fig. 5a). However, these concentrations in the laser-reduced regions were 87.77 wt% and 12.23 wt%, for C and O, respectively (Fig. 5b). This drastic reduction in the oxygen level indicates that a large number of oxygen-containing functional groups were removed from the original material by the laser treatment.

The laser-induced reduction process is a very fast, simple, chemical free, room temperature technique that exploits the thermal reactivity of GO. The photothermal effect was able to induce the conversion of GO into rGO, in agreement with the results previously reported by other researchers [41,42]. During the pulsed laser treatment of free standing GO paper, the absorbed laser

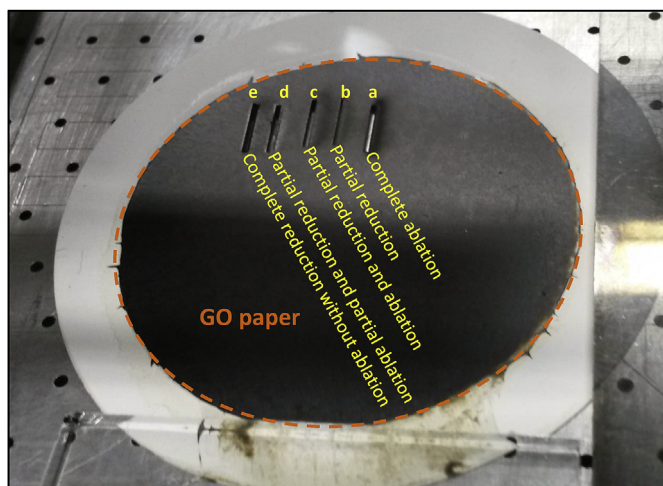


Fig. 4. Photograph of GO paper with laser tracks used for optimization of processing parameters. The optimum conditions for direct laser writing should be able to generate conductive rGO for electrodes. Track letters correspond to (a) = 365 mW; (b) = 310 mW; (c) = 340 mW; (d) = 335 mW and (e) = 325 mW laser power.

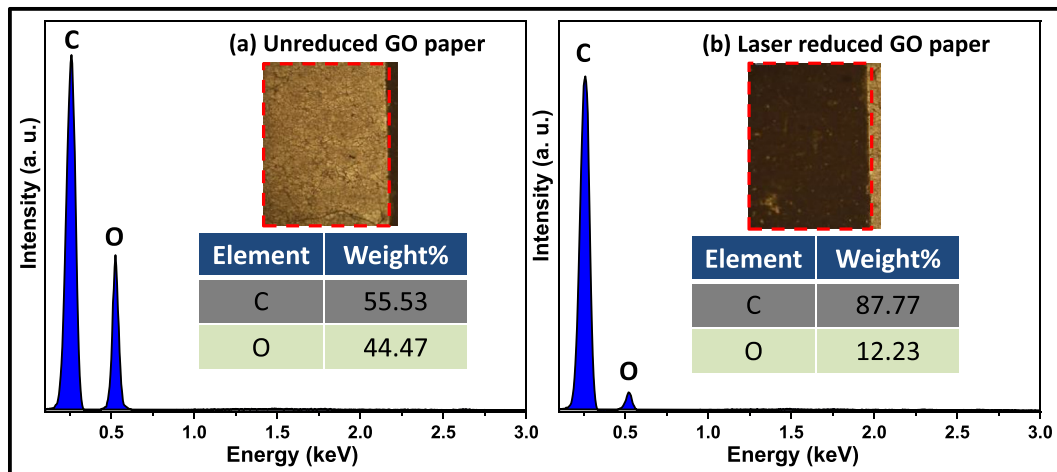


Fig. 5. (a) EDS spectra of (a) unreduced GO paper and (b) laser reduced GO paper (darker region).

energy was rapidly converted into heat on the sample surface, triggering the desorption of oxygen containing functional groups (mainly epoxy and hydroxyl at basal planes) [43]. For longer exposure times or higher laser power settings, thermal effects become more and more prominent, ultimately giving rise to photo-thermal breakdown of carbon-carbon bonds, creating lattice defects [44].

Optical images of laser-scribed GO paper are shown in Fig. 6. The electrodes of the μ -SCs are composed of equal numbers of “fingers” on each side, separated by insulating GO spacers which were not affected by the laser. Fig. 6a shows that the laser-reduced GO linear regions appear darker due to removal of oxygen containing functional groups from the GO paper. Fig. 6b and c shows that magnified rGO lines on both electrode sides are completely reduced without ablation from the incident laser energy. The laser treatment with optimized conditions achieved complete reduction of the GO paper right through its thickness.

One of the most important characterization tools for the structural investigation of carbon materials is Raman spectroscopy. The laser-reduced portions, after writing on GO paper, contain a large number of defects when compared to the unreduced portions, and this has been associated to changes in the Raman spectra. Fig. 7 shows the Raman spectra for both the laser treated portion (i.e. rGO) and the pristine GO paper. Two characteristic peaks from the carbon lattice can be noticed (the G and D bands) for unreduced and laser reduced GO paper [45]. The out-of-plane breathing mode of sp^2 atoms in graphite is responsible for the D band and the G band corresponds to the vibrations of sp^2 carbon atom domains of graphite. For unreduced GO paper (Fig. 7a), the D band is located at 1344 cm^{-1} and the G band at 1570 cm^{-1} . For the laser-reduced GO paper (Fig. 7b), both bands moved toward higher Raman shifts, now appearing at 1350 cm^{-1} (D band) and 1575 cm^{-1} (G band). The shift in peak position and the clear intensity variation of the D band confirm the generation of structural defects and the reduction

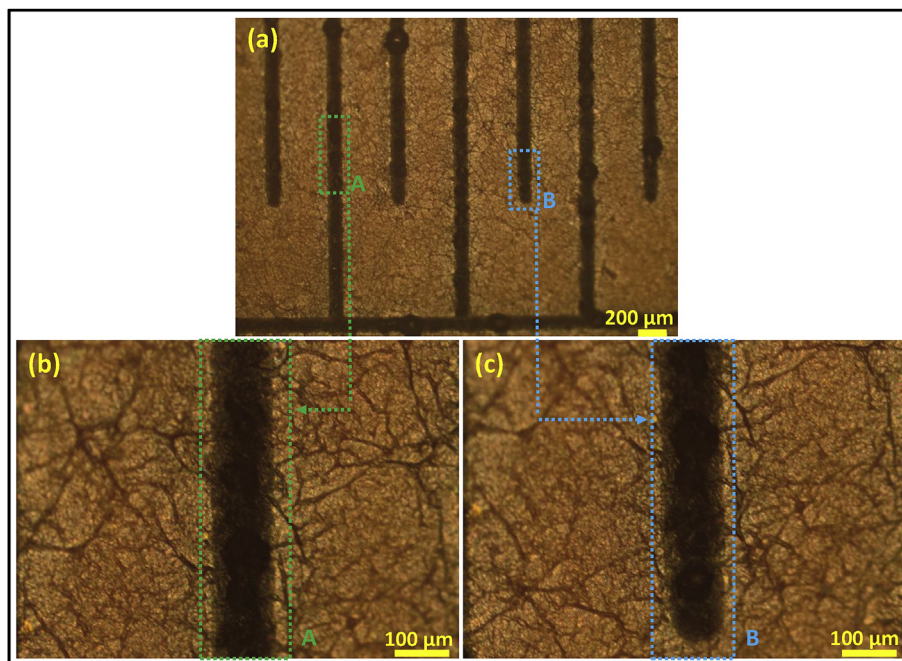


Fig. 6. Optical microscopy of laser treated GO paper. (a) Laser-written GO-rGO alternating pattern; (b,c) higher magnification of laser-reduced regions of opposite electrodes.

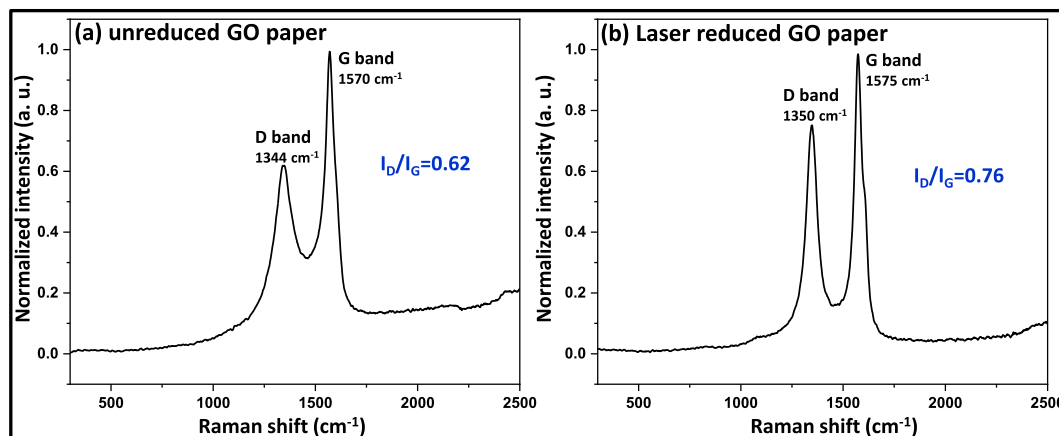


Fig. 7. Raman spectra of (a) unreduced GO paper and (b) laser-reduced GO paper.

imposed by direct laser writing. It is known that the ratio of peak intensities of the D band and the G band (I_D/I_G) indicates a deviation from the perfect honeycomb structure (e.g., defects, ripples and edges) for rGO. In our case, I_D/I_G increases from 0.62 for GO paper (Fig. 6a) to 0.76 for the laser reduced GO paper (Fig. 6b), indicating that most of the oxygen-containing functional groups from GO are being removed from its surfaces/edges during laser writing. The increase in the I_D/I_G ratio induced by the GO reduction process has also been reported elsewhere [46–48].

After successful fabrication of the μ -SCs, their electrochemical properties were evaluated by analysis of CV curves. The CV curves were acquired in the voltage range of 0–0.8 V at scan rates from 10 to 600 mV/s and the lower scan rates (up to 90 mV/s) are shown in Fig. 8. Two kinds of electrolytes, KOH and NaCl, with the same molarity (1 M) were used to study the electrochemical performance of the μ -SCs. The same device was used in the measurements which were carried out in the following order: (i) pristine μ -SC (Fig. 8a, as-fabricated μ -SC, without electrolyte), (ii) with KOH electrolyte (Fig. 8b, interdigitated area was covered by KOH solution), (iii) after removing KOH electrolyte (Fig. 8c, after removing KOH solution and drying) and (iv) with NaCl electrolyte (Fig. 8d, interdigitated area was covered by NaCl solution).

It can be observed in the results for the pristine μ -SC (Fig. 8a) that the CV curves are nearly straight lines and all the loops enclose very small areas (resistive behavior). With increasing scan rates, only small changes in loop area were found. After filling the region between the electrodes with the first electrolyte (KOH solution), a large increase in current was observed and the graphs exhibited nearly rectangular shapes, indicating capacitive behavior (Fig. 8b). CV curve areas were progressively bigger with increasing scan rates. After removing the KOH electrolyte and drying (Fig. 8c), the CV curves again showed nearly straight lines and the loops enclosed very small areas, similar to those seen in Fig. 8a (pristine μ -SC). The small areas are due to the ions available in the unreduced portion which lies between the “fingers” formed by the laser-reduced (rGO) conducting portion. The fabricated μ -SC was then tested with NaCl electrolyte, and the obtained CV curves (Fig. 8d) illustrated an increase in the current as the scan rate was increased. The CV curves for both KOH and NaCl electrolytes exhibited nearly rectangular shape, without any peaks, indicating that the μ -SCs exhibited capacitive behavior due to the presence of rGO. These findings reveal that the μ -SCs exhibit electric double-layer capacitance and can be used with different electrolytes without changes in the internal morphology.

The CV testing was performed at several scan rates and the areal

capacitance (C , in F/cm^2) was calculated from equation (1) [49]:

$$C = \int \frac{idV}{Av\Delta V} \quad (1)$$

where i is the current (A), v is the scan rate (V/s), ΔV is the potential window (V) and A is the area of interdigitated electrodes (cm^2) for μ -SCs on free standing GO paper. Using data from the CV curves measured at various scan rates, the areal capacitance of μ -SCs was calculated for each situation, and the results are shown in Fig. 9. At the low scan rate of 10 mV/s, the areal capacitances (in $\mu F/cm^2$) were 0.08 for pristine μ -SCs without any electrolyte, 9.3 with KOH electrolyte, 0.05 after removing the KOH solution and drying, and 13.8 with NaCl electrolyte. For the higher scan rate (600 mV/s), the μ -SCs displayed areal capacitances of 3.1 and 3.5 $\mu F/cm^2$ with KOH and NaCl electrolytes, respectively. The enhanced electrochemical behavior in CV measurements, especially at low scan rates, can be attributed to the ions provided by the electrolytes. The calculated areal capacitance from CV curves (13.8 $\mu F/cm^2$ using 1 M NaCl) is higher than for other reported SCs devices. For example, Gao et al. reported flexible solid-state graphene SCs with a capacitance of 12.4 $\mu F/cm^2$ [50]. Soam et al. achieved 13 $\mu F/cm^2$ areal capacitance by using on-chip μ -SCs based on silicon nanowires [15].

Another crucial parameter for the performance of μ -SCs in practical situations is the long-term cycling stability. Cycling performance testing of μ -SCs was carried out by repeating the CV curves for 3400 cycles at a scan rate of 90 mV/s (in 1 M NaCl electrolyte). One can observe in the results shown in Fig. 10a that after an initial loss in the first cycles, a negligible loss in the capacitance value of interdigitated μ -SCs occurs during the remainder of the test. The capacitance retention tends to a steady state after about 62 cycles, with the CV curves keeping the same shape and maintaining 95.1% of the initial capacitance value, showing excellent stability.

The electrochemical charge/discharge performance of the μ -SCs was analyzed in the potential range from 0 to 0.8 V (vs. Ag/AgCl) using two electrode systems in 1 M NaCl electrolyte (Fig. S1: Supporting information). The shapes of the charge/discharge curves gradually become more triangular for higher currents, indicating that the electrode has nearly capacitive characteristics with electrochemical reversibility. EIS measurements were conducted to investigate the charge transfer and ion diffusion characteristics of μ -SCs. The EIS measurements were performed in a two-electrode system using a signal with amplitude of 5 mV over a frequency range from 0.1 Hz to 100 kHz. Fig. 10b shows the Nyquist plot for μ -SCs in 1 M NaCl electrolyte. In the high frequency region, the value of the intercept at the real axis (Z') represents the equivalent series

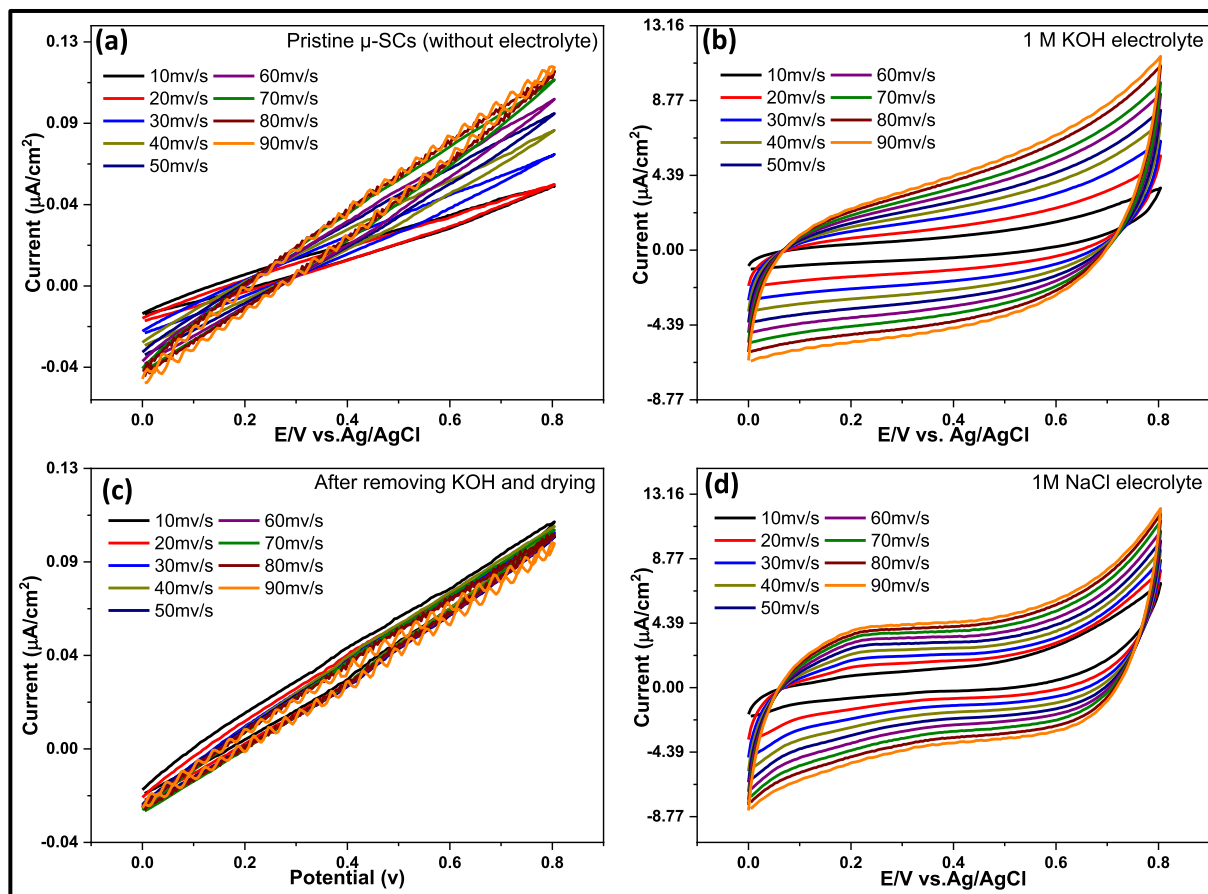


Fig. 8. CV curves of μ -SCs at various scan rates in different electrolytes. (a) Pristine μ -SCs (without electrolyte), (b) KOH electrolyte, (c) after removing the electrolyte and drying, (d) NaCl electrolyte.

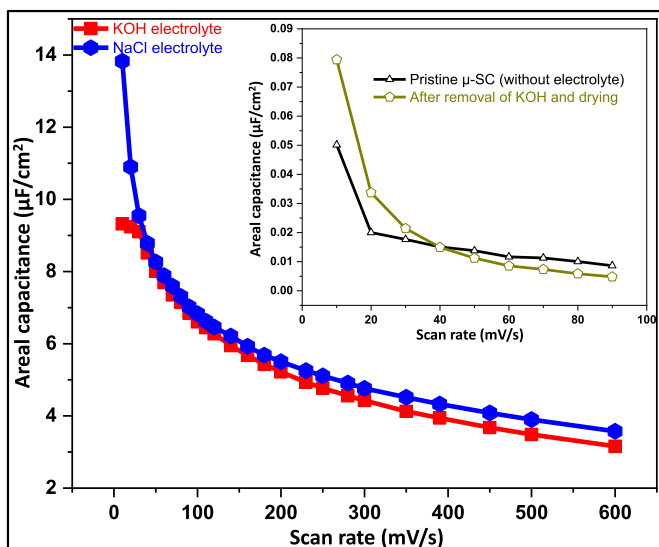


Fig. 9. Areal capacitance of μ -SCs (with and without electrolytes) as a function of the different scan rates used for testing.

resistance ($R_s \sim 2\Omega$), including the ionic resistance of electrolyte, internal resistance of substrate and active material, and contact resistance at the active material/current collector interface [51,52]. The semicircle across high and mid-frequencies is attributed to the

charge-transfer resistance (R_{ct}) at the interface between the interdigitated electrode and the electrolyte solution. The Nyquist plot for the μ -SC shows a small R_{ct} value ($\sim 6\Omega$), another indication of the good electrochemical performance.

Table 1 shows published results of measurements performed by other authors on μ -SCs/SCs fabricated by direct laser writing on GO/carbon based film sheets/papers. The results obtained in this work are also included in the last row of the table. Direct comparisons are difficult due to the different materials, dimensions, electrolytes, testing conditions and properties reported.

4. Conclusions

We have fabricated μ -SCs via the mask-free method by direct laser writing on GO paper. By using a pulsed UV laser, the reduction of GO paper generated high-quality rGO in thin conducting lines, which could be drawn to form electrodes without the need for additional operations. The technique is fast, flexible and cost effective, not requiring any masks, photolithography, transfer and post-processing, chemical treatments, controlled atmospheres, vacuum systems, high temperature treatments or stringent clean room operations. The thin GO paper is very flexible and easily foldable, opening the possibility for increasing volumetric power density. These characteristics are also compatible with emerging applications in foldable and wearable devices. The open, layered structures in the laser-treated regions of GO paper are well-suited for ionic and electronic exchange, with a highly increased availability of electrochemically active sites/interfaces. The fabricated μ -

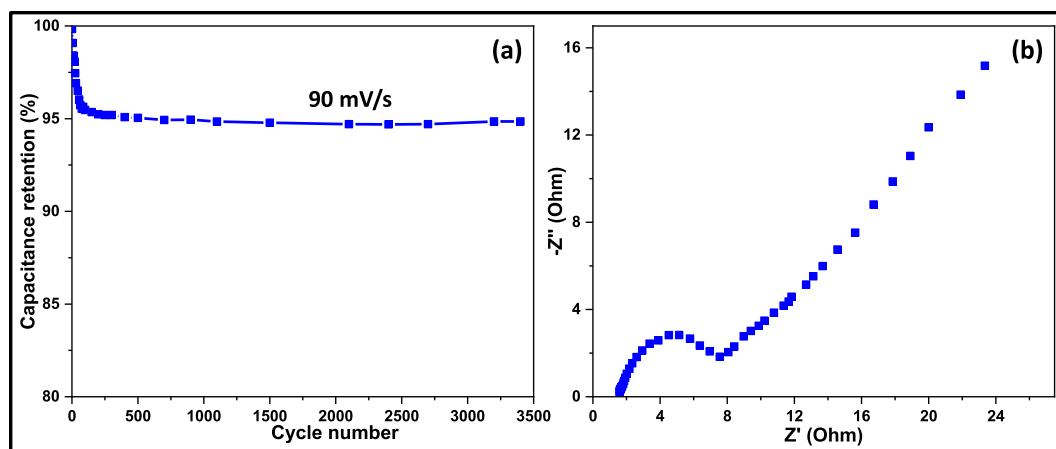


Fig. 10. Long-term cycling stability in NaCl electrolyte and (b) Nyquist plot of fabricated μ -SCs tested in NaCl electrolyte.

Table 1

Comparison of published results from direct laser writing on GO/carbon based films/sheets/papers for fabrication of μ -SCs/SCs and their electrochemical performance.

Type of laser	Laser parameters (power: P; scan speed: s; wavelength: λ)	Film/paper/electrode thickness	Electrolyte	Capacitance/capacitive retention of SCs/ μ -SCs	Ref.
CO ₂ laser	P = 2.4 W s = 30% máx.	hydrated GO films (~22 μ m)	1 M Na ₂ SO ₄ /1 M TEABF ₄ in CH ₃ CN	0.51 mF/cm ² ; 80% (first half hour) and 50% (period of 8 h)	[29]
CO ₂ laser	P = 3.6 W; s = 88.9 mm/s; λ = 10.6 μ m	polyimide film (127 μ m)	1 M H ₂ SO ₄ /BMIM-BF ₄	4 mF/cm ² (20 mV/s)	[53]
CO ₂ laser	P = 4.8 W	polyimide film (127 μ m)	PVA/H ₂ SO ₄	9.11 mF/cm ² (0.01 mA/cm ²)	[54]
CO ₂ laser	P = 2 W	GO film (~8 μ m)	polymeric gel electrolyte	82–107 F/g (0.1–1.0 mA/cm ²); 95% (2000 cycles)	[55]
CO ₂ laser	P = 4.8–5.2 W; λ = 10.6 μ m	mushroom-derived carbon (7 μ m)	PVA/H ₂ SO ₄ gel electrolyte	12.92 F/cm ³ ; 90% (1000 bending cycles)	[56]
CO ₂ laser	—	polyimide film/MnO ₂	gel electrolyte	1.7 F/cm ³ (10 mV/s); 84% (10,000 cycles)	[12]
Nanosecond UV laser	P = 1–2 W; s = 5 m/s; λ = 355 nm	PET film/Ni/graphene oxide	LiCl-PVA gel electrolyte	3.9 mF/cm ² (0.25 mA/cm ²)	[57]
Infrared laser	P = 5 mW; λ = 788 nm	GO film (~7.6 μ m)	1 M H ₂ SO ₄	4.04 mF/cm ² (1 A/g); 97% (10,000 cycles)	[58]
Nd:YVO ₄ pulsed UV laser	P = 244 mW; s = 2.5 mm/s; λ = 355 nm	ultra-thin GO film (2.2 μ m)	0.1 M Na ₂ SO ₄	106 μ F/cm ² (0.3 V/s); 92.5% (5000 cycles)	[32]
Nd:YVO ₄ pulsed UV laser	P = 310 mW; s = 2.0 mm/s; λ = 355 nm	GO thick film (4.0 μ m)	0.1 M NaOH	2.40 μ F/cm ² (50 mV/s); 93.1% (3500 cycles)	[33]
Nd:YVO ₄ pulsed UV laser	P = 325 mW; s = 2.0 mm/s; λ = 355 nm	GO paper (10 μ m)	1 M NaCl	13.8 μ F/cm ² (10 mV/s); 95.1% (3400 cycles)	This work

SCs reached an areal capacitance of 13.8 μ F/cm² and displayed long-term charge cycling stability, with 95.1% capacitance retention after 3400 cycles. The devices could be used with different electrolytes without any structural damage or defects from irreversible reactions. This study provides new data into the reduction process of GO paper using a technique which opens doors to a high degree of flexibility and control in the fabrication of graphene-based devices. Direct laser-assisted reduction of GO paper could be used to prepare structures having different shapes, containing devices with controlled concentrations of oxygen functional groups for specific applications.

Acknowledgements

R.K. acknowledges the Japan Society for the Promotion of Science, Japan for prestigious international postdoctoral fellowship (Standard: P18063), and financial supports (JSPS KAKENHI Grant No. 18F18063 and JSPS KAKENHI Grant No.18H03841). Authors E.J. R.S. and S.A.M. would like to acknowledge FAPESP, CNPq and CAPES (Brazilian funding agencies) for financial support. Also, this work was partially supported by FAPESP (2017/22186-0 and 2013/14262-7) and CNPq, Brazil.

Appendix A. Supplementary data

Supplementary data to this article can be found online at <https://doi.org/10.1016/j.energy.2019.05.032>.

References

- [1] Iqbal MF, Ashiq MN, Hassan M-U, Nawaz R, Masood A, Razaq A. Excellent electrochemical behavior of graphene oxide based aluminum sulfide nanowalls for supercapacitor applications. *Energy* 2018;159:151–9.
- [2] Kumar R, Kim H-J, Park S, Srivastava A, Oh I-K. Graphene-wrapped and cobalt oxide-intercalated hybrid for extremely durable super-capacitor with ultra-high energy and power densities. *Carbon* 2014;79:192–202.
- [3] Kumar R, Joanni E, Singh RK, Singh DP, Moshkalev SA. Recent advances in the synthesis and modification of carbon-based 2D materials for application in energy conversion and storage. *Prog Energy Combust Sci* 2018;67:115–57.
- [4] Ensafi AA, Ahmadi N, Rezaei B, Abdolmaleki A, Mahmoudian M. A new quaternary nanohybrid composite electrode for a high-performance supercapacitor. *Energy* 2018;164:707–21.
- [5] Kumar R, Singh RK, Dubey PK, Singh DP, Yadav RM. Self-assembled hierarchical formation of conjugated 3D cobalt oxide nanobead-CNT-graphene nanostructure using microwaves for high-performance supercapacitor electrode. *ACS Appl Mater Interfaces* 2015;7(27):15042–51.
- [6] Kumar R, Singh RK, Vaz AR, Savu R, Moshkalev SA. Self-assembled and one-step synthesis of interconnected 3D network of Fe₃O₄/reduced graphene oxide nanosheets hybrid for high-performance supercapacitor electrode. *ACS Appl Mater Interfaces* 2017;9(10):8880–90.
- [7] Yadav SK, Kumar R, Sundramoorthy AK, Singh RK, Koo CM. Simultaneous

- reduction and covalent grafting of polythiophene on graphene oxide sheets for excellent capacitance retention. *RSC Adv* 2016;6(58):52945–9.
- [8] Li J, Shi Q, Shao Y, Hou C, Li Y, Zhang Q, et al. Cladding nanostructured AgNWs-MoS₂ electrode material for high-rate and long-life transparent in-plane micro-supercapacitor. *Energy Storage Materials* 2019;16:212–9.
- [9] Bivio MA, Acosta GG, Kessler T, Visintin A. Flexible symmetric and asymmetric supercapacitors based in nanocomposites of carbon cloth/polyaniline - carbon nanotubes. *Energy* 2017;130:22–8.
- [10] Pourjavadi A, Doroudian M, Ahadpour A, Pournadiei B. Preparation of flexible and free-standing graphene-based current collector via a new and facile self-assembly approach: leading to a high performance porous graphene/polyaniline supercapacitor. *Energy* 2018;152:178–89.
- [11] Hu H, Pei Z, Ye C. Recent advances in designing and fabrication of planar micro-supercapacitors for on-chip energy storage. *Energy Storage Materials* 2015;1:82–102.
- [12] Huang Z, Yuan B. All-solid-state pseudocapacitive micro-supercapacitors from laser-treated polymer derivatives. *Chin Chem Lett* 2018;29(4):596–8.
- [13] Kim S-W, Kang K-N, Min J-W, Jang J-H. Plotter-assisted integration of wearable all-solid-state micro-supercapacitors. *Nano Energy* 2018;50:410–6.
- [14] Wu Z-S, Parvez K, Feng X, Müllen K. Photolithographic fabrication of high-performance all-solid-state graphene-based planar micro-supercapacitors with different interdigital fingers. *J Mater Chem* 2014;2(22):8288–93.
- [15] Soam A, Arya N, Singh A, Dusane R. Fabrication of silicon nanowires based on-chip micro-supercapacitor. *Chem Phys Lett* 2017;678:46–50.
- [16] Yao L, Cheng T, Shen X, Zhang Y, Lai W, Huang W. Paper-based all-solid-state flexible asymmetric micro-supercapacitors fabricated by a simple pencil drawing methodology. *Chin Chem Lett* 2018;29(4):587–91.
- [17] Liu F, Yang X, Qiao Z, Zhang L, Cao B, Duan G. Highly transparent 3D NiO-Ni/Ag-nanowires/FTO micro-supercapacitor electrodes for fully transparent electronic device purpose. *Electrochim Acta* 2018;260:281–9.
- [18] Shi X, Zeng Z, Liao C, Tao S, Guo E, Long X, et al. Flexible, planar integratable and all-solid-state micro-supercapacitors based on nanoporous gold/manganese oxide hybrid electrodes via template plasma etching method. *J Alloy Comp* 2018;739:979–86.
- [19] Sun G, An J, Chua CK, Pang H, Zhang J, Chen P. Layer-by-layer printing of laminated graphene-based interdigitated microelectrodes for flexible planar micro-supercapacitors. *Electrochem Commun* 2015;51:33–6.
- [20] Huang P, Pech D, Lin R, McDonough JK, Brunet M, Taberna P-L, et al. On-chip micro-supercapacitors for operation in a wide temperature range. *Electrochem Commun* 2013;36:53–6.
- [21] Pech D, Brunet M, Taberna P-L, Simon P, Fabre N, Mesnilgrente F, et al. Elaboration of a microstructured inkjet-printed carbon electrochemical capacitor. *J Power Sources* 2010;195(4):1266–9.
- [22] Ye W, Yumeng S, Cheng Xi Z, Jen It W, Xiao Wei S, Hui Ying Y. Printed all-solid flexible microsupercapacitors: towards the general route for high energy storage devices. *Nanotechnology* 2014;25(9):094010.
- [23] Kim S-K, Koo H-J, Lee A, Braun PV. Selective wetting-induced micro-electrode patterning for flexible micro-supercapacitors. *Adv Mater* 2014;26(30):5108–12.
- [24] Xue M, Xie Z, Zhang L, Ma X, Wu X, Guo Y, et al. Microfluidic etching for fabrication of flexible and all-solid-state micro supercapacitor based on MnO₂ nanoparticles. *Nanoscale* 2011;3(7):2703–8.
- [25] Wu Z-S, Parvez K, Li S, Yang S, Liu Z, Liu S, et al. Alternating stacked graphene-conducting polymer compact films with ultrahigh areal and volumetric capacitances for high-energy micro-supercapacitors. *Adv Mater* 2015;27(27):4054–61.
- [26] Brousse K, Huang P, Pinaud S, Respaud M, Daffos B, Chaudret B, et al. Electrochemical behavior of high performance on-chip porous carbon films for micro-supercapacitors applications in organic electrolytes. *J Power Sources* 2016;328:520–6.
- [27] Li Y-Q, Shi X-M, Lang X-Y, Wen Z, Li J-C, Jiang Q. Remarkable improvements in volumetric energy and power of 3D MnO₂ microsupercapacitors by tuning crystallographic structures. *Adv Funct Mater* 2016;26(11):1830–9.
- [28] Tong QC, Luong MH, Rimmel J, Do MT, Nguyen DTT, Lai ND. Rapid direct laser writing of desired plasmonic nanostructures. *Opt Lett* 2017;42(12):2382–5.
- [29] Gao W, Singh N, Song L, Liu Z, Reddy ALM, Ci L, et al. Direct laser writing of micro-supercapacitors on hydrated graphite oxide films. *Nat Nanotechnol* 2011;6:496.
- [30] Cai J, Lv C, Watanabe A. Laser direct writing of high-performance flexible all-solid-state carbon micro-supercapacitors for an on-chip self-powered photodetection system. *Nano Energy* 2016;30:790–800.
- [31] El-Kady MF, Kaner RB. Scalable fabrication of high-power graphene micro-supercapacitors for flexible and on-chip energy storage. *Nat Commun* 2013;4:1475.
- [32] Kumar R, Savu R, Joanni E, Vaz AR, Canesqui MA, Singh RK, et al. Fabrication of interdigitated micro-supercapacitor devices by direct laser writing onto ultra-thin, flexible and free-standing graphite oxide films. *RSC Adv* 2016;6(88):84769–76.
- [33] Kumar R, Joanni E, Singh RK, da Silva ETSG, Savu R, Kubota LT, et al. Direct laser writing of micro-supercapacitors on thick graphite oxide films and their electrochemical properties in different liquid inorganic electrolytes. *J Colloid Interface Sci* 2017;507:271–8.
- [34] Kumar R, Singh RK, Singh DP, Joanni E, Yadav RM, Moshkalev SA. Laser-assisted synthesis, reduction and micro-patterning of graphene: recent progress and applications. *Coord Chem Rev* 2017;342:34–79.
- [35] Wang X, Kuchmizhak AA, Brasselet E, Juodkazis S. Dielectric geometric phase optical elements fabricated by femtosecond direct laser writing in photore-sists. *Appl Phys Lett* 2017;110(18):181101.
- [36] Papazoglou S, Tsouti V, Chatzandroulis S, Zergioti I. Direct laser printing of graphene oxide for resistive chemosensors. *Optic Laser Technol* 2016;82:163–9.
- [37] Aguilar-Morales AI, Alamri S, Kunze T, Lasagni AF. Influence of processing parameters on surface texture homogeneity using direct laser interference patterning. *Optic Laser Technol* 2018;107:216–27.
- [38] Hummers WS, Offeman RE. Preparation of graphitic oxide. *J Am Chem Soc* 1958;80(6):1339.
- [39] Koch KR. Oxidation by Mn2O7: an impressive demonstration of the powerful oxidizing property of dimanganeseheptoxide. *J Chem Educ* 1982;59(11):973.
- [40] Dreyer DR, Park S, Bielawski CW, Ruoff RS. The chemistry of graphene oxide. *Chem Soc Rev* 2010;39(1):228–40.
- [41] Lazauskas A, Marcinauskas L, Andrulevicius M. Photothermal reduction of thick graphene oxide multilayer films via direct laser writing: morphology, structural and chemical properties. *Superlattice Microsc* 2018;122:36–45.
- [42] Petridis C, Lin Y-H, Savva K, Eda G, Kymakis E, Anthopoulos TD, et al. Post-fabrication, in situ laser reduction of graphene oxide devices. *Appl Phys Lett* 2013;102(9):093115.
- [43] Cote LJ, Cruz-Silva R, Huang J, Flash reduction and patterning of graphite oxide and its polymer composite. *J Am Chem Soc* 2009;131(31):11027–32.
- [44] Chichkov BN, Momma C, Nolte S, von Alvensleben F, Tünnermann A. Femtosecond, picosecond and nanosecond laser ablation of solids. *Appl Phys A* 1996;63(2):109–15.
- [45] Kumar R, Singh RK, Dubey PK, Singh DP, Yadav RM, Tiwari RS. Freestanding 3D graphene-nickel encapsulated nitrogen-rich aligned bamboo like carbon nanotubes for high-performance supercapacitors with robust cycle stability. *Advanced Materials Interfaces* 2015;2(15):1500191.
- [46] Bo Z, Shuai X, Mao S, Yang H, Qian J, Chen J, et al. Green preparation of reduced graphene oxide for sensing and energy storage applications. *Sci Rep* 2014;4:4684.
- [47] Sadhukhan S, Ghosh TK, Rana D, Roy I, Bhattacharyya A, Sarkar G, et al. Studies on synthesis of reduced graphene oxide (RGO) via green route and its electrical property. *Mater Res Bull* 2016;79:41–51.
- [48] Feng Y, Feng N, Du G. A green reduction of graphene oxide via starch-based materials. *RSC Adv* 2013;3(44):21466–74.
- [49] Brousse K, Nguyen S, Gillet A, Pinaud S, Tan R, Meffre A, et al. Laser-scribed Ru organometallic complex for the preparation of RuO₂ micro-supercapacitor electrodes on flexible substrate. *Electrochim Acta* 2018;281:816–21.
- [50] Gao Y, Zhou YS, Xiong W, Jiang LJ, Mahjouri-samani M, Thirugnanam P, et al. Transparent, flexible and solid-state supercapacitors based on graphene electrodes. *Apl Mater* 2013;1(1):012101.
- [51] Mi W, Dai C, Zhou S, Yang J, Li Q, Xu Q. Chemical precipitation synthesis of KCoF₃ for supercapacitor applications. *Mater Lett* 2018;227:66–9.
- [52] Zhu T, Wang J, Ho GW. Self-supported yolk-shell nanocolloids towards high capacitance and excellent cycling performance. *Nano Energy* 2015;18:273–82.
- [53] Lin J, Peng Z, Liu Y, Ruiz-Zepeda F, Ye R, Samuel ELG, et al. Laser-induced porous graphene films from commercial polymers. *Nat Commun* 2014;5:5714.
- [54] Peng Z, Lin J, Ye R, Samuel ELG, Tour JM. Flexible and stackable laser-induced graphene supercapacitors. *ACS Appl Mater Interfaces* 2015;7(5):3414–9.
- [55] Ghoniem E, Mori S, Abdel-Moniem A. Low-cost flexible supercapacitors based on laser reduced graphene oxide supported on polyethylene terephthalate substrate. *J Power Sources* 2016;324:272–81.
- [56] Yadav P, Basu A, Suryawanshi A, Game O, Ogale S. Highly stable laser-scribed flexible planar microsupercapacitor using mushroom derived carbon electrodes. *Advanced Materials Interfaces* 2016;3(11):1600057.
- [57] Xie B, Wang Y, Lai W, Lin W, Lin Z, Zhang Z, et al. Laser-processed graphene based micro-supercapacitors for ultrathin, rollable, compact and designable energy storage components. *Nano Energy* 2016;26:276–85.
- [58] El-Kady MF, Strong V, Dubin S, Kaner RB. Laser scribing of high-performance and flexible graphene-based electrochemical capacitors. *Science* 2012;335(6074):1326–30.